Fragmentation Patterns of Radiosensitizers Metronidazole and Nimorazole Upon Valence Ionization

Eero Itälä,* Johannes Niskanen,* Lassi Pihlava, and Edwin Kukk*

Department of Physics and Astronomy, University of Turku, FI-20014, Finland

E-mail: eero.itala@utu.fi; johannes.niskanen@utu.fi; edwin.kukk@utu.fi

Abstract

We study gas-phase photodissociation of radiosensitizer molecules nimorazole and metronidazole with the focus on the yield of oxygen mimics nitrogen oxides and nitrous acid. Regardless of photon energy, we find nimorazole cation to split the intramolecular bridge with little NO_2 or NO production, which makes the molecule a precursor of dehydrogenated methylnitroimidazole. Metronidazole cation, on the contrary, has numerous fragmentation pathways with strong energy dependence. Most notably, ejection of NOOH and NO_2 take place within 4 eV from the valence ionization energy. Whereas the NO_2 ejection is followed by further fragmentation steps when energy so allows, we find emission of NOOH to take place in microsecond time-scales, and as a slow process to be relevant only when no other competing reaction is feasible. These primary dissociation characteristics of the molecules are understood by applying the long-known principle of rapid internal conversion of the initial electronic excitation energy, and by studying the energy minima and the saddle points on the potential energy surface of the electronic ground state of the molecular cation.

Introduction

A number of recent studies of nitroimidazoles using mass and electron spectroscopic techniques[1–10] have been motivated by the success in using some nitroimidazoles in combination with radiation therapy to increase its effect.[11–13] Nimorazole in particular has proven to be a useful radiosensitizer and is being used in the treatment of certain head and neck cancers in Denmark.[14] The benefit of using nitroimidazoles as radiosensitizers arises mostly in the case of hypoxic tumors (low oxygen concentration), which are more resistant to ionizing radiation than well-oxynated tumors.[15]

Despite the success of nitroimidazole-based compounds as radiosensitizers, the fundamental mechanism of how these compounds act as radiosensitizers is yet to be established. Nitroimidazoles are commonly regarded as oxygen mimetics that undergo enzymatic and

radiation-induced redox reactions.[16,17] Under irradiation by ionizing radiation, nitroimidazoles produce agents that falsely fix (*cf.* oxygen fixation hypothesis) DNA radical lesions in a hypoxic environment. In a recent study on free and hydrated nimorazole, Denifl *et al.* discovered that nimorazole has a high electron attachment cross-section and that virtually the only dissociative electron attachment process is the loss of NO_2.[2] Solvation seemed to effectively block the dissociative electron attachment processes, and thus their conclusion was that one of the key factors in radiosensitization by nitroimidazoles is the effective free radical anion formation by low-energy electron collisions.[2] Ionization and radical formation by secondary electron collisions commonly occur in radiotheraphy following the initial photoionization and they can be expected to play an important role in the radiation-induced redox reactions.

In this paper, we present a valence photoionization study of two nitroimidazole derivatives, nimorazole and metronidazole (see Figure 1). While nimorazole has a side chain with a morpholine group at the end, creating a double-ring structure, metronidazole has a linear side chain. As NO_2 is a strong oxidizer and NO is considered to be an effective radiosensitizer,[18] we focus mainly on the yield of these compounds and investigate the hypothesis that high yield of NO_2 and/or NO is associated with the radiosensitizing effect of nitroimidazoles.

Although both metronidazole and nimorazole have been widely studied clinically as potential radiosensitizers, only nimorazole has been found to be useful for this purpose.[17,19] Studies on isolated nimorazole suggest that when subjected to ionization, nimorazole dissociates easily. The photoionization threshold for nimorazole is also lower compared to other similar compounds, such as 4(5)-nitroimidazole or 1-methyl-5-nitroimidazole.[9]

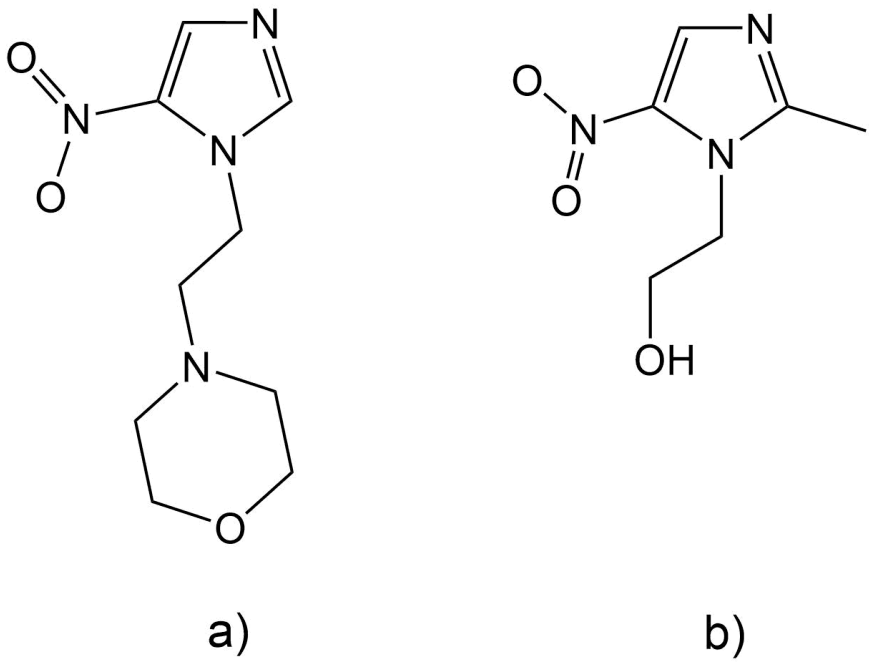

Figure 1: The skeletal structures of the studied samples. Nimorazole (a) has a morpholine group (C_4H_8NO) attached to the 5-nitroimidazole structure by an ethyl bridge (-C_2H_2-). Metronidazole (b) consists of 5-nitroimidazole with ethenol (C_2H_4OH) and methyl group (CH_3) attached to the imidazole ring.

Methods

Experiment

We carried out the measurements using a PhotoElectron-PhotoIon COincidence (PEPICO) setup described in detail elsewhere.[20] The setup consists of an electron spectrometer (Omicron 150 mm mean radius hemispherical analyzer, equipped with a 40 mm active area microchannel plate and resistive anode position sensitive detector) and a Wiley-McLaren ion time-of-flight (ToF) spectrometer. The electron spectrometer was set to operate at 50 eV pass energy using a 1 mm entrance slit and was tuned to monitor the kinetic energy window from 6.3 to 14 eV with the electron energy resolution of 200 meV. The ion spectrometer was operated under the Wiley-McLaren focussing conditions with the drift tube potential of -727 V and the ion extraction voltage of 200 V (applied as pulsed $\pm$100 V across the source region). In addition to the electron triggers from the electron detector, ions were also

extracted by independently generated "random" triggers in order to evaluate and subtract the false coincidence contributions. For recording non-coincident ion ToF spectra, pulsed extraction at about 5 kHz rate was used.

To ionize the sample molecules we used a gas-discharge lamp with He, Ar or Xe gas for photon energy of 21.22 eV, 11.62 eV (11.83 eV) and 8.43 eV (9.57 eV) of the main (secondary) lines, respectively.[21] The photon bandwidth of these emission lines is in the order of a few meV,[22] negligible compared to the electron energy resolution. The lack of high-energy components in the Ar and Xe emission spectra was confirmed by the lack of N_2 and O_2 ionization (a trace amount of O_2^+ ions was detected with Ar emission lines).

We used an effusion cell to introduce the metronidazole (purchased from Sigma-Aldrich with stated purity of $\geq$99%) and the nimorazole (purchased from Adooq Bioscience with stated purity of $\geq$98%) samples to the experimental chamber. The heating temperature was kept at around 65°C for metronidazole and 90°C for nimorazole to avoid thermal degradation. With metronidazole, we took special care to keep the temperature sufficiently low, as thermal degradation became notable already at 70°C. With nimorazole, the situation was easier as no evidence of thermal degradation at temperatures well above 100°C was observed in our experiments.

Model and Simulations

After ionization by the ultraviolet (UV) light, the cation may be left in an excited electronic state. We applied the approximation of immediate internal conversion of electronic excitation energy to kinetic energy of the nuclei by vibronic coupling. In this framework, dissociation processes occur on the electronic ground state energy surface of the cation and are driven by the aforementioned energy converted from the initial electronic excitations. We thus simplify the complicated problem to a study of energy minima, saddle points, and dissociation limits of this potential energy surface.

For a theoretical prediction for dissociation energetics, we carried out geometry optimiza-

tions for the neutral molecule, for the cation and for chosen fragments. We then searched the transition state (TS) along a path from the cationic geometry to a fragmented one prepared from geometries of the optimized fragments. For this we utilized nudged elastic band (NEB) transition state search methods (NEB-TS) and its climbing-image version (NEB-CI) in cases where the former search failed. We utilized the ORCA 4.2.0 software[23] for all calculations.

To model the electronic structure and energetics, we applied unrestricted Kohn-Sham (UKS) density functional theory (DFT) with the Perdew–Burke–Ernzerhof (PBE)[24] exchange-correlation potential. We used the def2-TZVP basis set[25] and the def2/J auxiliary basis set[26] for the applied resolution of identity (RI-J) approximation. We ran all simulations for radicals with the KDIIS algorithm, and to overcome convergence issues in the self-consistent field (SCF) procedure we used additional dampening and level shifting. In addition, the Kohn-Sham Fock matrix was fully rebuilt on every SCF iteration.

Experimental Results

Nimorazole

The mass spectra of nimorazole measured with 8.43 eV, 11.62 eV and 21.22 eV photons are presented in Fig. 2. Already the 8.43 eV photons cause ionization, which is consistent with the photoelectron spectroscopy study by Feketeová *et al.*[8] As Fig. 2 indicates, increasing the photon energy does not significantly increase the variety of ion fragments; the dissociation is strongly characterized by $C_5H_{10}NO^+$ (100 u). The observed cationic fragments are listed in Table 1.

Metronidazole

Whereas the fragmentation scheme of nimorazole is simple and straightforward, dissociation of metronidazole is quite the opposite. As the mass spectrum of Fig. 3 and the list of fragments of Table 2 show, ionization of metronidazole induces a large number of different

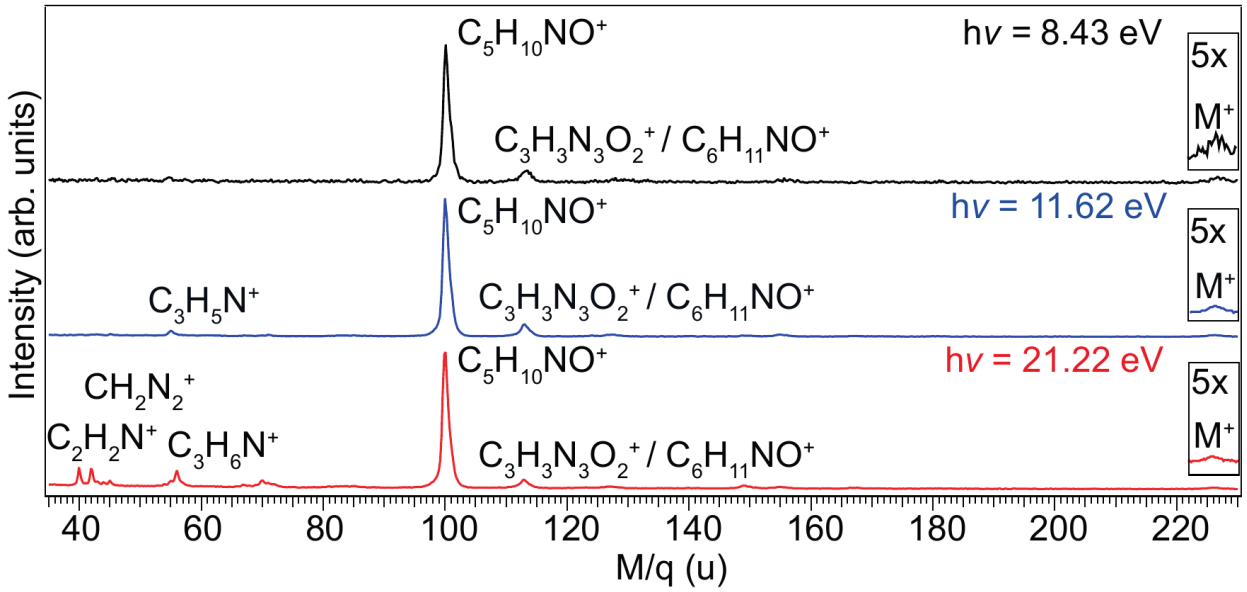

Figure 2: Ion mass spectra of nimorazole measured with 8.43 eV, 11.62 eV and 21.22 eV photons.

Table 1: Ion fragments following the ionization of nimorazole following 8.43 eV, 11.62 eV and 21.22 eV ionization. The intensities are given with respect to the strongest mass peak.

M (u)	Fragments	Relative intensity		
		8.43 eV	11.62 eV	21.22 eV
226	M^+	0.11	0.02	0.01
113	$C_3H_3N_3O_2^+$ $C_6H_{11}NO^+$	0.14	0.11	0.07
100	$C_5H_{10}NO^+$	1.00	1.00	1.00
56	$C_3H_6N^+$			0.09
55	$C_3H_5N^+$		0.02	
42	$CH_2N_2^+$			0.03
40	$C_2H_2N^+$			0.04

dissociation channels. Therefore, instead of using three different photon energies, we applied the PEPICO method to study the fragmentation and its energetics in greater detail.

We present the PEPICO data as a false-color map (Fig. 4) that depicts the detected coincident electron-ion count rate as a function of the electron binding energy (BE) and the ion ToF. In the map, the detected ionic fragments of a particular mass-to-charge ratio appear as horizontal lines. The length of the lines and their positioning along the x-axis

indicates the range of electron BEs over which the fragment is produced. The number of ionic fragments observed in the PEPICO measurement is lower than that in the non-coincident mass spectrum of Fig. 3, since the latter contains fragments from ionization of the inner valence orbitals with the BE up to the photon energy of 21.22 eV, whereas the BE range of the PEPICO map is determined by the electron spectrometer, in this particular case from 8.0 eV to 14.7 eV.

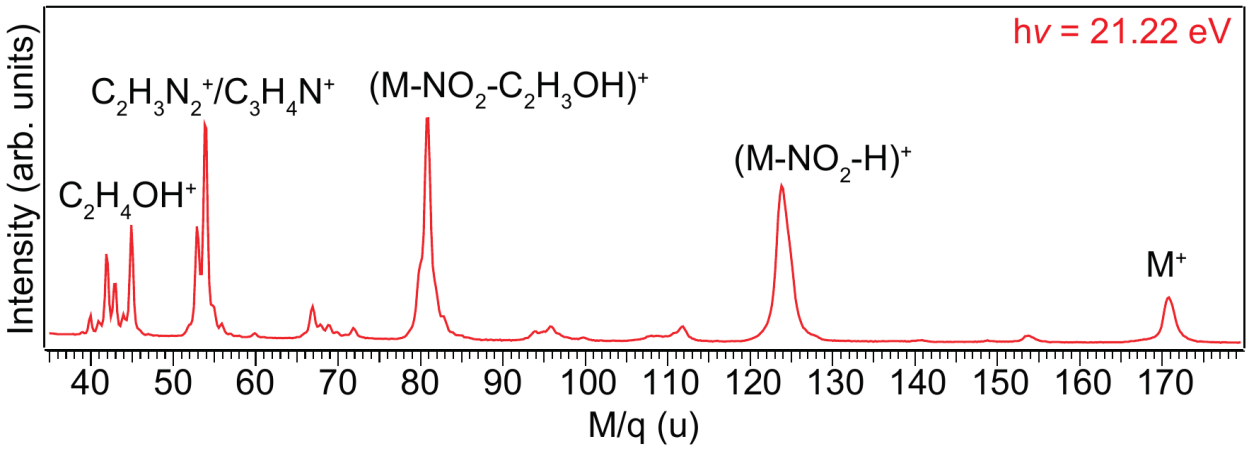

Figure 3: Ion mass spectrum of metronidazole measured with 21.22 eV photons.

Ionization deeper in the valence leaves the cationic system in an excited electronic state, with an opportunity to convert the excess energy to the nuclear subsystem by internal conversion. Therefore knowledge of the coincident electron BE from PEPICO allows for studies of the internal-energy dependence of fragmentation patterns. In particular, this technique allows for the determination of the appearance energies (AE) of observed fragmentation products from the onset of their horizontal ion line. We determined the AEs as described in Ref.,[27] by extracting coincident ion yield curves corresponding to each mass peak. Even though the $[M-NOOH]^+$ and $[M-NOO]^+$ (124 u and 125 u, respectively) peaks are overlapping in the ToF scale, the PEPICO map of Figure 4 shows that these fragments are formed in clearly separate energy regions, which allows the determination of AEs also for these fragments. Figure 5 (left) presents ToF spectra integrated over selected electron binding energy ranges. Ions in coincidence with $E_b = 9.9 - 10.5$ eV and $E_b = 10.9 - 11.6$ eV photoelectrons

correspond to the M=124 u fragment, and ions in coincidence with the $E_b = 12.2 - 13.4$ eV electrons correspond to the M=125 u fragment. Figure 5 (right) shows the branching ratio curves obtained from the heights of the two gaussian curves obtained from stepwise (0.25 eV) proceeding fit with line-shape parameters fixed from the gaussian fit of the $E_b = 10.9$-11.6 eV (M=124 u) and $E_b = 12.2$ - 13.4 eV (M=125 u) regions. The false coincidence contribution was subtracted.

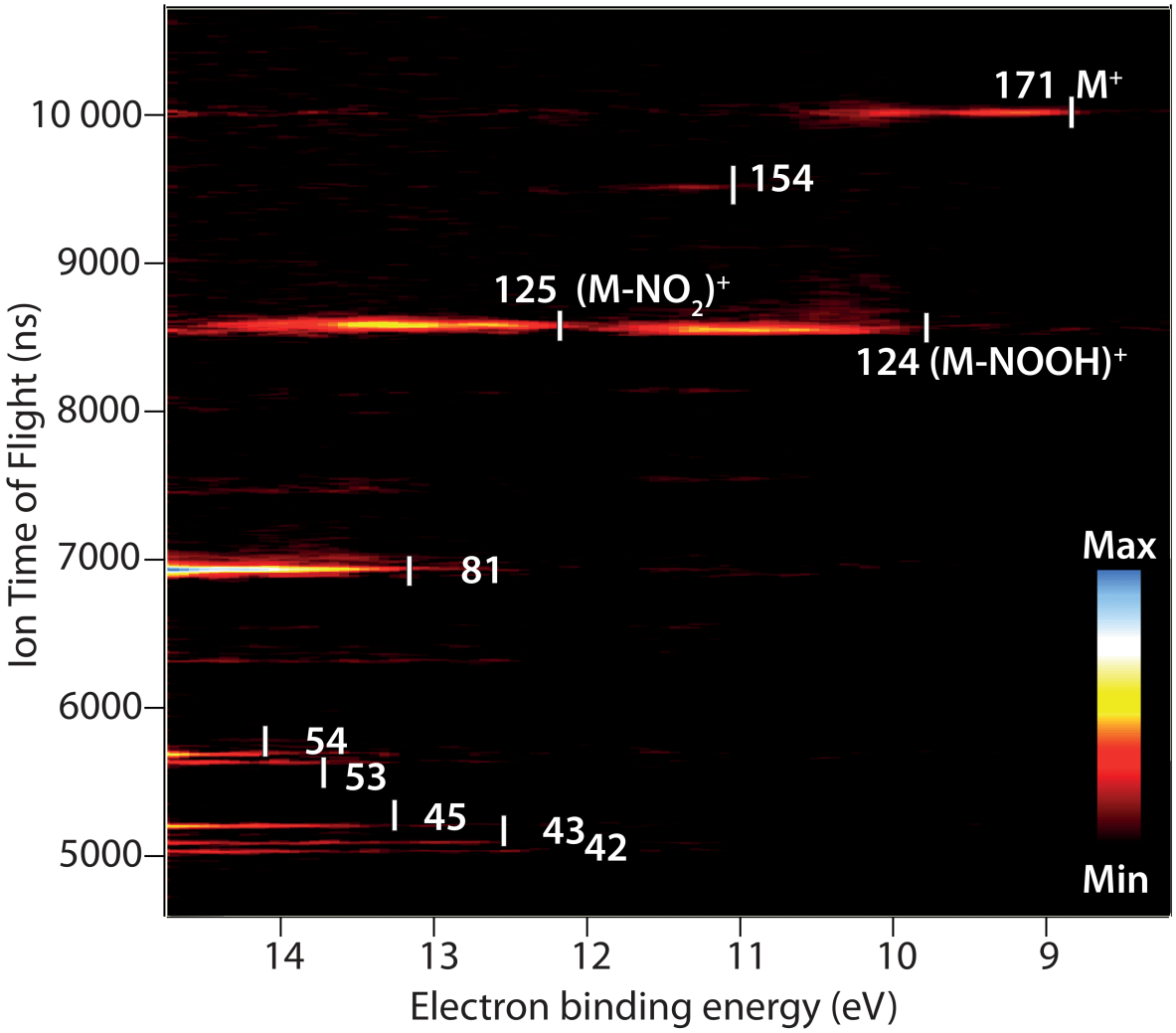

Figure 4: PEPICO map of metronidazole measured with 21.22 eV photons. The color scale is set to start above zero to cut the background noise. The small white bars denote the AE for each fragment.

The AE for the metronidazole parent molecule gives the first ionization potential of the

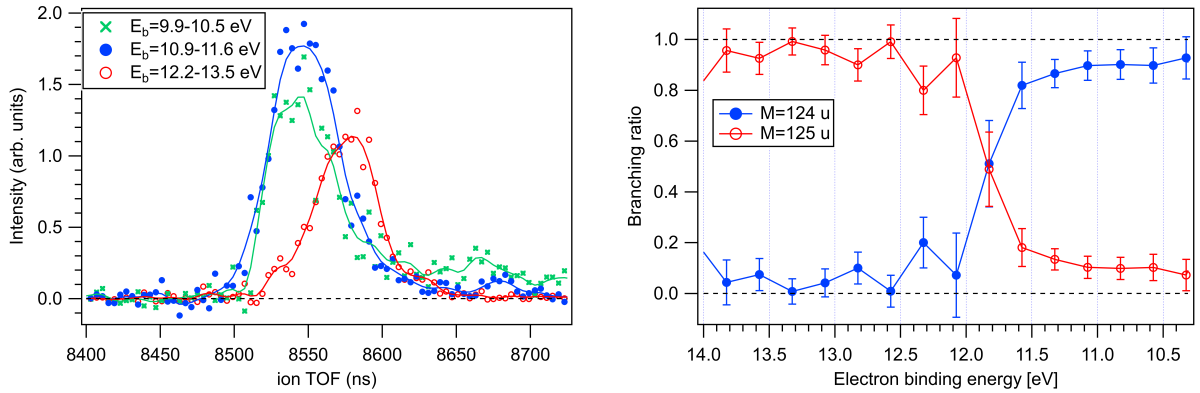

Figure 5: Left panel: Ion ToF peaks of the $[M-NOOH]^+$(124 u) and $[M-NOO]^+$(125 u) fragments, detected in coincidence with the photoelectron in a given binding energy range as shown in the legend. Continuous lines are a guide to the eye connecting the data points. The peak corresponding to the lowest binding energy range shows the asymmetric contribution from metastable parent decay. The contribution from false coincidences was subtracted using ion TOF spectra measured with generated (not electron) triggers. Right panel: Branching ratios of the two fragments as a function of the binding energy of the coincident electron.

molecule at 8.76 eV (Fig. 4 and Table 2). The parent cation remains stable with increasing BE (and the internal energy) in a relatively long range of about 1 eV, after which the threshold for neutral NOOH release is reached. At 12.19 eV, the NO_2 release replaces the NOOH ejection, and more extensive fragmentation begins slightly above this BE.

The PEPICO map shows two distinct signs of a long-lived (microseconds) parent cation at the NOOH emission threshold around 10 eV BE. Firstly, the high-ToF tail for the $[M-NOOH]^+$ feature in Fig. 4 originates from the parent cation dissociating during its acceleration in the spectrometer (see also ion spectrum coincident with $E_b = 9.9 - 10.5$ eV electrons in Fig 5). In such a case, some of the potential energy due to the electric field is used for accelerating the heavier M^+ ion, which results in lower-than-expected velocity and longer-than-expected ToF for the lighter $[M-NOOH]^+$ fragment. Secondly, if the dissociation of the parent occurs even later, in the field-free drift tube, the $[M-NOOH]^+$ ions reach the detector at the ToF of the M^+ parent ion with an additionally broadened ToF profile, clearly observable in the M^+ feature at around 10 eV BE. This broadening is due to the kinetic energy released in the dissociation, and is missing from the ToFs of the stable M^+ at

lower BEs.

Table 2: Ionic fragments following the ionization of metronidazole by 21.22 eV photons. Appearance energies are given for the fragments present in the PEPICO map.

M (u)	Fragment	AE
171	M^+	8.76±0.14
154	$(M\text{-}OH)^+$	11.03±0.19
141	$(M\text{-}NO)^+$	
125	$(M\text{-}NO_2)^+$	12.19±0.15
124	$(M\text{-}NOOH)^+$	9.81±0.13
112	$(M\text{-}C_2H_3OH\text{-}CH_3^+)$	
96	$(M\text{-}NO\text{-}C_2H_3OH)^+$	
94	$(M\text{-}NO_2\text{-}CH_2OH)^+$	
82	$(M\text{-}NO_2\text{-}C_2H_2OH)^+$	
81	$(M\text{-}NO_2\text{-}C_2H_3OH)^+$	13.15±0.18
80	$(M\text{-}NO_2\text{-}C_2H_4OH)^+$	
67	$(M\text{-}NO_2\text{-}C_2H_4OH\text{-}CH_3)^+$	
54	$C_2H_2N_2^+/C_3H_4N^+$	14.13±0.23
53	$C_2HN_2^+/C_3H_3N^+$	13.77±0.59
45	$C_2H_4OH^+$	13.27±0.52
43	$C_2H_2OH^+$	12.63±0.41
42	$C_2HOH^+/C_2H_4N^+$	

Discussion

Nimorazole

Figure 6 presents a dissociation chart of nimorazole. Once ionized, the molecule nearly always dissociates via the formation of the $C_5H_{10}NO^+$ (100 u) fragment. The figure also presents our suggestion for the few weak fragmentation channels that explain the minor fragments of nimorazole. Since the fragmentation is so clearly dominated by the formation of $C_5H_{10}NO^+$ via the separation of the ring structures, we limit the discussion to only this fragmentation channel.

We simulated the fragmentation process producing $C_5H_{10}NO^+$. Figure 7 represents a straightforward bond cleavage pathway (NEB-CI) of nimorazole into $C_5H_{10}NO^+$ and

$C_4H_4N_3O_2$ moieties via a barrier 0.46 eV above the vertical ionization potential (VIP). The match in the numerical values for TS and the dissociation limit (DL; calculated as two separate fragments with integer charges) is accidental, although indicative of a flat energy landscape.

The simulated bond cleavage process supports the experimental findings well. Firstly, it is energetically easy for cationic nimorazole to dissociate into $C_5H_{10}NO^+$ (the dominant fragment ion) and $C_4H_4N_3O_2$. Secondly, although the parent mass peaks are weak, the parent ion is present in all spectra of Fig. 2. This indicates that there is a stable cationic local minimum (CLM) state for the parent molecule. Our calculation identifies such a CLM, lower than the VIP and the TS. Thirdly, the experiment indicates that once the molecule has enough energy for $C_5H_{10}NO^+$ and $C_4H_4N_3O_2$ formation, it follows this fragmentation pathway regardless of further increase of energy. We understand this to be owing to simplicity of the C−C-bond-cleavage pathway; minimal number of chemical bond breakdowns (*i.e.* energy) is required with this straightforward transition pathway.

The somewhat dull scheme of the UV-induced fragmentation of nimorazole is interesting from the viewpoint of radiosensitization, as this established radiosensitizer molecule does not show NO_2 or NO release. Therefore, in addition to NO_2 or NO production in the gas phase, there are mechanisms that can be associated with the radiosensitizing properties of nitroimidazoles. However, amongst the produced fragments of nimorazole, dehydrogenated 1-methyl-5-nitroimidazole (DMeNIZ) is likely. We note that a comparable molecule 5-nitroimidazole (5-NIZ) is known to produce NO_2 and $NO^{(+)}$ upon secondary fragmentation.[3] Based on this evidence, the hypothetical nitrogen-oxide-based mechanism for radiosensitization would rely on further dissociation of the DMeNIZ and 5-NIZ, with an additional ionization event.

However, the effects of the chemical environment or slight structural alterations could be unpredictable. For example, the study of Pandeti *et al.*[5] shows that protonation may alter the fragmentation characteristics of nimorazole notably. While protonation also produces the $C_5H_{10}NO^+$ fragment, its yield is reduced and a new process, ejection of neutral 5-

nitroimidazole, begins to dominate the fragmentation. In addition, another, weaker new process opens up due to protonation, the formation of $C_4H_9NO^+$.

Metronidazole

Metronidazole has a potential energy landscape rich of possible structures owing to the relatively easy conformation of the C_2H_4OH tail and its interaction with NO_2 group. The molecule also shows a variety of fragments with a strong energy-dependence of their yields. In the used model for the lowest NOOH and NO_2 release pathways (see Fig. 8), the metronidazole molecule is first photoionized above the VIP, after which any electronic excitation energy is converted immediately to the nuclear subsystem in the electronic ground state of the cation. The structure shown for neutral system is the lowest-energy one that we found, and sound in terms of OH... ONO hydrogen bonding. Along the transition path a CLM, lower in energy than the VIP and the TS, is found in agreement with the observation of a stable parent ion. At the TS, the C_2H_2OH tail attacks the ring to form a double ring structure, the formation of which compensates for the energy required for breakdown of the C−N bond (a new C−O bond is formed). The DL was calculated as two separate fragments. However, given enough energy the requirement for the second ring closure may also be lifted, and thus the path for NO_2 ejection may become more straightforward and rapid. A similar argument for NOOH emission is not valid, as the attack of the C_2H_4OH tail is required for hydrogen transfer.

For emission of both NOOH and NO_2, a coordinated attack of the ethanol tail at the C-N bond is required, which may limit the reaction rate notably. As a result, long-lived species may be expected, even though energy alone would allow for dissociation. We interpret this to be in line with the observed long lifetime, in the microsecond range, of the parent cation at the internal energies close to the AE of the $[M-NOOH]^+$ (electron BE around 10 eV). We also note that there was no such experimental evidence (ToF tails) for other dissociation channels, which indicates that fragmentation along other, higher-appearance-energy pathways occurs

more quickly.

As observed in the experiment, the NOOH release is found to be energetically more favourable than the NO_2 release in our calculations. The simulated AE of 9.14 eV for $[M-NOOH]^+$ agrees fairly well with the experimental value of 9.81 eV, whereas for $[M-NO_2]^+$ the obtained value of 9.85 eV is notably lower than the experimental one (12.19 eV). This over-2-electronvolt deviation is far beyond errors typically observed in density-functional simulations, and we conclude that this path is not taken. To explain the high AE of $[M-NO_2]^+$, we investigated a scenario where the NO_2 group is removed from the parent cation as the first step along the dissociation pathway. The final geometry of the $[M-NOO]^+$ fragment of this "direct NO_2 ejection" pathway, shown in Figure 9, was obtained by optimization starting from the cationic VIP structure from which the NO_2 group was removed. The direct NO_2 emission is followed by H transfer from the tail to the ring as the second step, and as a result a more straightforward stepwisely proceeding transition path is obtained. Here the TS search proved to be difficult and we ended up using the NEB-CI formalism with which the TS of energy 11.30 eV was obtained, in a better agreement with the experimental value 12.19 eV.

The simulation also provides insight into fragmentation processes different from the NOO emission. The experimental observation of the 81-u cationic fragment is hinted by the structure of the $[M-NO_2]^+$ cation resulting from the "direct NOO ejection" pathway calculation. Here the removal of the remaining C_2H_3OH tail would be a straightforward process. Owing to the H transfer step, the lowest-energy explanation for the observation of $C_2H_4OH^+$ is rather via a direct ejection from the parent cation than via a back-transfer of a proton. With higher internal energies, ejection of $C_2H_4OH^+$ is also foreseeable from the TS of Figure 9.

As a synthesis of the observations, we constructed a pathway chart for the photofragmentation of metronidazole, presented in Fig. 10. We consider the dissosiation outcome to be dictated by the internal energy (and the BE of the photoelectron) as follows: below the

BE of 12.19 eV, the NOOH ejection path and above the 12.19 eV, the NO_2 path is taken. In the latter, hydrogen transfer from the tail to the ring follows the NO_2 emission. Above the BE of 13.15 eV, the NO_2-emission path can be continued further by the separation of the remaining C_2H_3OH (45 u) tail from the $C_4N_2H_5^+$ ring. Finally, the $C_4N_2H_5^+$ ring may dissociate above the BE of 14.13 eV to a charged fragment of M=54 u or smaller with numerous possible formulas. As an example we consider two possible structures with M=54 that are obtained by cutting a bond that in neutral molecule was formally a double bond. The presented chart accounts for the observation of positive fragments 125 u, 81 u, 54 u, and 45 u with a minimal number of required bond breakdowns and in increasing order of energy. We note that from $[M-NOOH]^+$ a reaction chain similar to that of $[M-NO_2]^+$ would require additional transfers of protons over several bonds. Since the $[M-NOOH]^+$ primary channel is overrun by NO_2 emission where energetically feasible, and since it has a long lifetime, we consider the path to be relevant only for low BEs where no competing mechanism is possible.

Upon bombardment with X-rays or other energetic particles, radiation damage is mainly induced by secondary electrons more numerous than the incident particles. As a collision chain proceeds from its primary event, valence ionization by electrons becomes a likely mechanism: each collision-ionization event produces two slower electrons for one faster incident electron. Because fragmentation processes with lower energy thresholds are available for more electrons, they are more likely. For metronidazole as a radiosensitizer, this logic renders the release of NOOH more probable than that of NO_2. However, since the NO_2 radical is more reactive than NOOH, its higher release-threshold may explain why metronidazole has been found to be a rather ineffective radiosensitizer.[17,28]

Similarly to nimorazole, also the fragmentation of metronidazole changes due to protonation. According to the study of Pandeti *et al.*,[5] protonated metronidazole most likely ejects a vinyl alcohol (C_2H_3OH tail), subsequently followed by NO_2 release. Also NO_2 release accompanied with the ejection of methyl group is possible, but less probable. Thus in the case of metronidazole, protonation seems to change the fragmentation tendency from NOOH

release to the ejection of the vinyl alcohol tail.

Conclusions

Fragmentation of isolated nimorazole and metronidazole molecules subsequent to valence photoionization follow quite different schemes – while nimorazole dissociates predominantly via a single fragmentation path, metronidazole exhibits a rich ensemble of fragmentation pathways. This difference is understood by the double ring structure of nimorazole, with a bridge highly susceptible for bond cleavage.

We applied density functional theory calculations for the energetics of the cation to explain the observed fragmentation pathways. These simulations were carried out in the nudged elastic band framework, which proved useful for both finding and identifying the transition states of the primary dissociation steps.

With little internal energy, the metronidazole cation dissociates relatively slowly via NOOH release, the experiment being consistent with microsecond-scale lifetimes. When the internal energy increases, NOOH release is quenched by a rapid NO_2 production at around 12.19 eV above the ground state. Due to the cascadic nature of radiation-energy deposition, processes that require the least energy are the most probable ones in living tissue. Thus, assuming similar fragmentation pathways than in the gas phase, NOOH release would be enhanced (and NO_2 release weakened) *in vivo* when compared to the conditions of this work. As NOOH is less reactive than the NO_2 radical, this may in turn explain the observed ineffectiveness of metronidazole as a radiosensitizer.

The good radiosensitizing properties of nimorazole, on the other hand, may be explained by the production of dehydrogenated 1-methyl-5-nitroimidazole and 5-nitroimidazole. These species are known to form a high yield of an effective radiosensitizer $NO^{(+)}$ and a strong oxidizer NO_2. Thus, the effectiveness of nimorazole as a radiosensitizer would originate from the molecule being a precursor for potent nitroimidazole radiosensitizers.

Acknowledgements

We acknowledge the financial support by the Academy of Finland (project no. 295551).

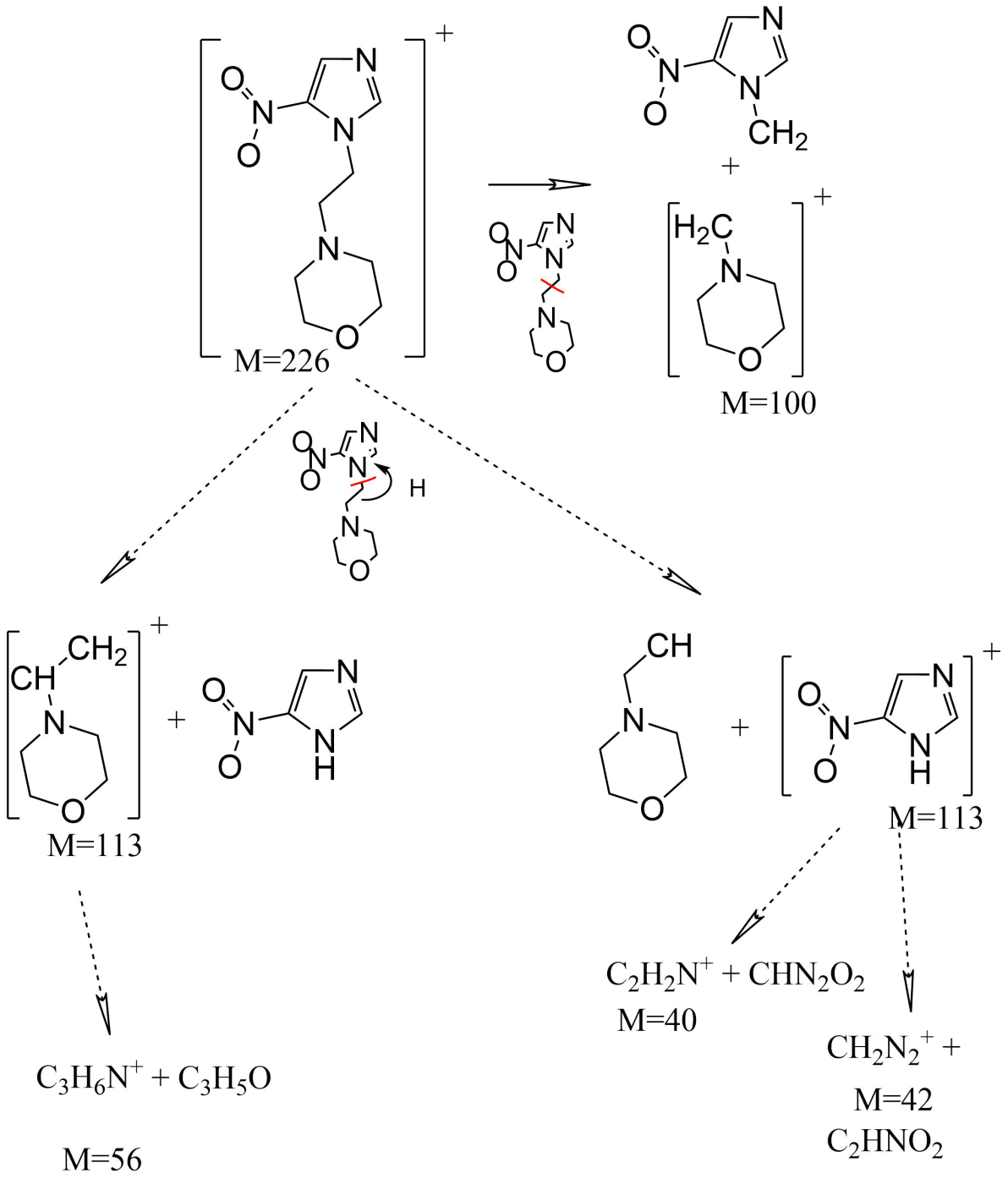

Figure 6: All fragmentation pathways of nimorazole following valence photoionization. Dashed arrows indicate minor pathways.

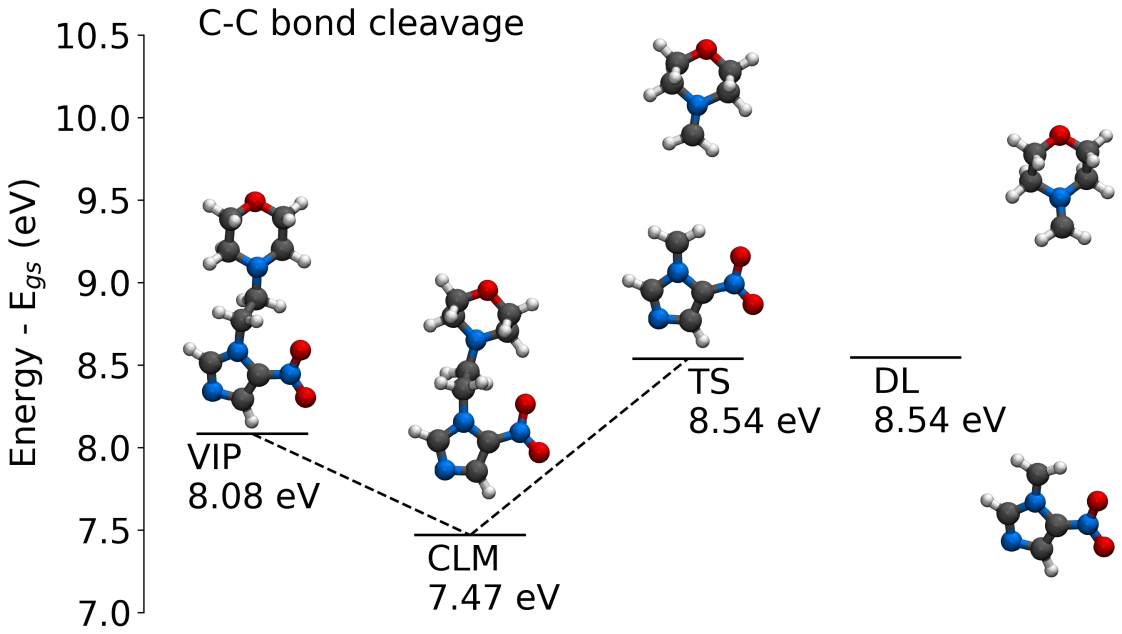

Figure 7: Fragmentation pathway of nimorazole to $C_5H_{10}NO^+$ and $C_4H_4N_3O_2$ by C-C bond cleavage from simulations. The energies of the vertical ionization potential (VIP), of the cationic local minimum (CLM), of the transition state (TS) and of the dissociation limit (DL) are shown relative to the neutral ground state.

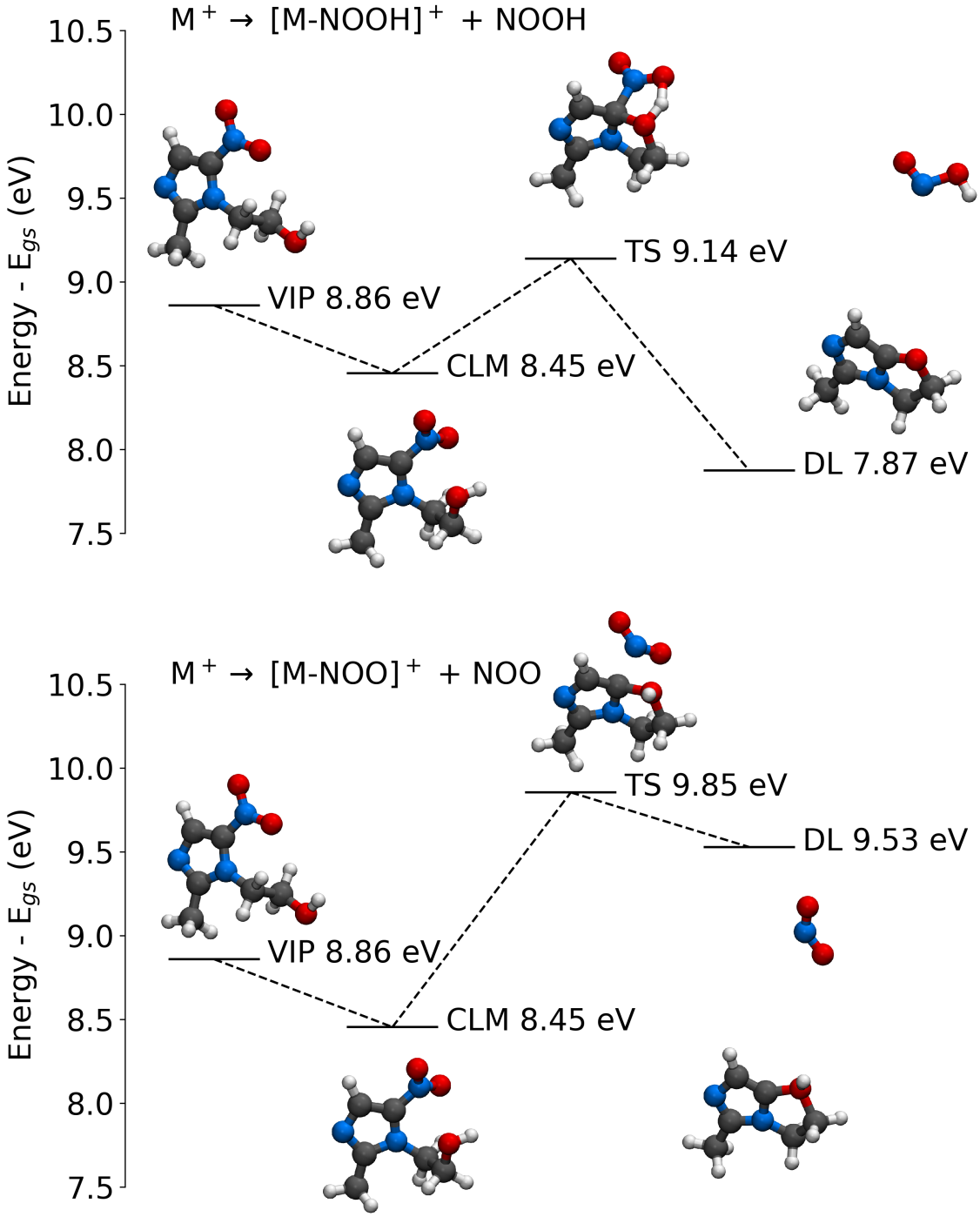

Figure 8: Simulated minimum-energy fragmentation pathways of NOOH and NO_2 ejection processes, shown in the left and right panel, respectively. The latter is not observed in the experiment. The energies of the vertical ionization potential (VIP), of the cationic local minimum (CLM), of the transition state (TS) and of the dissociation limit (DL) are shown relative to the neutral ground state.

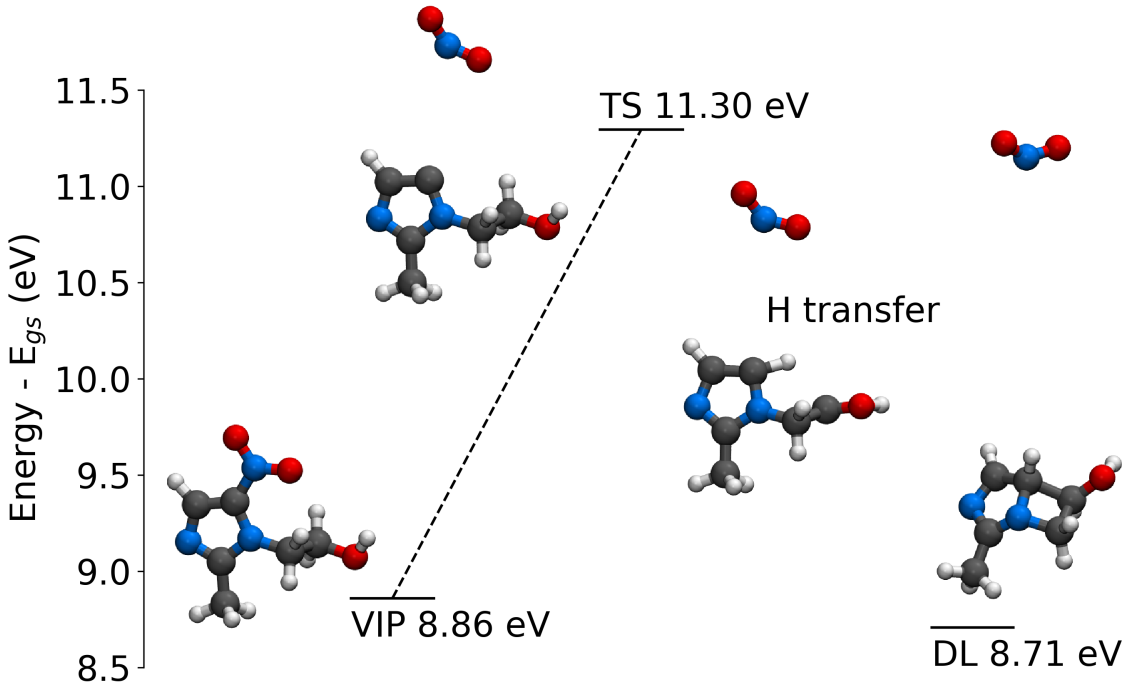

Figure 9: Simulated minimum-energy fragmentation pathway for the "direct NO_2 ejection" process.The energies of the vertical ionization potential (VIP), of the transition state (TS) and of the dissociation limit (DL) are shown relative to the neutral ground state.

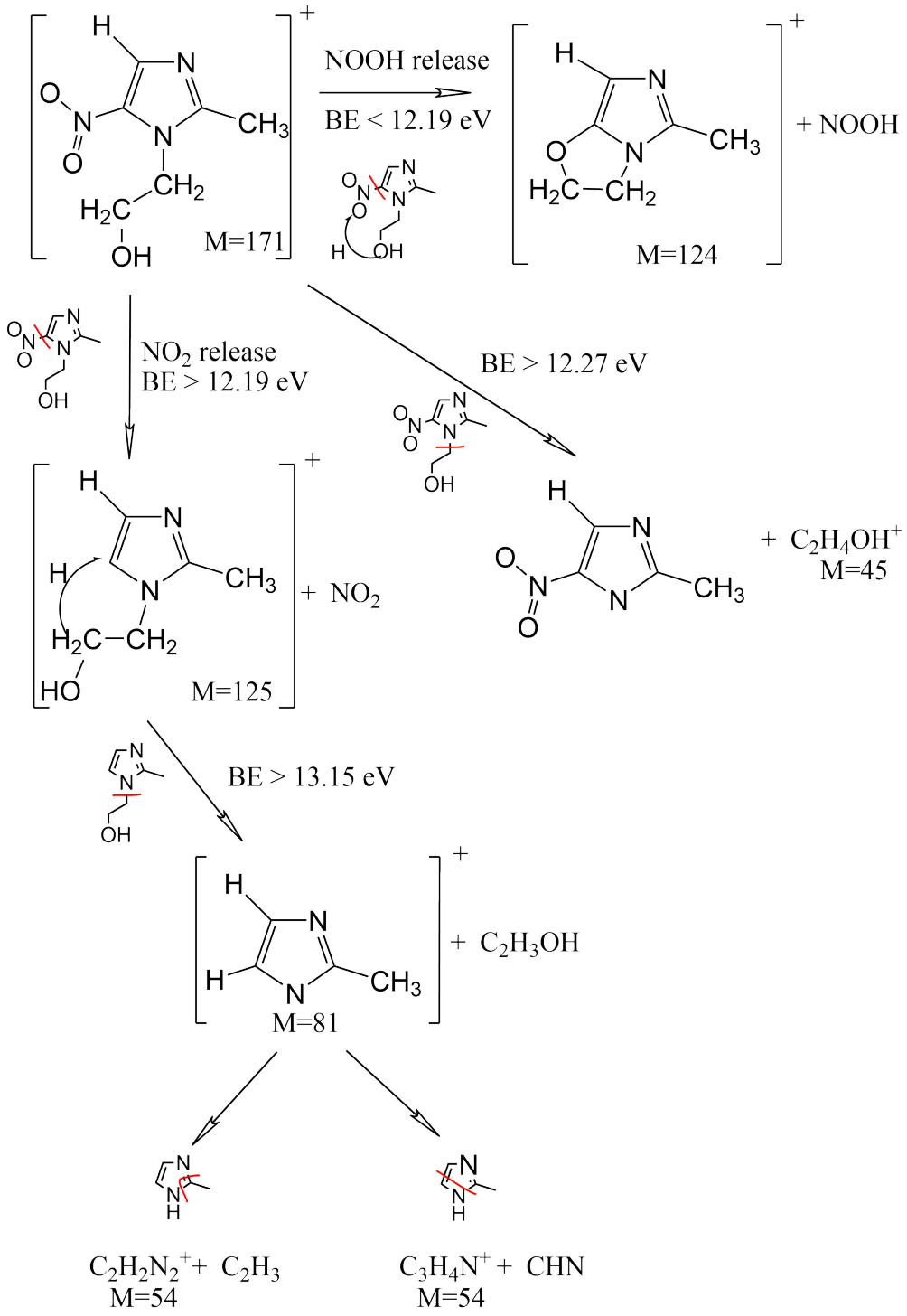

Figure 10: The dominant fragmentation pathways of metronidazole following valence photoionization. The pathways of several small fragments are not presented as the possible number of such fragmentation channels would be quite large. The smaller fragments observed in the experiment can be obtained by splitting the ring further.

References

(1) Mendes, M.; García, G.; Bacchus-Montabonel, M.-C.; Limão-Vieira, P. Electron Transfer Induced Decomposition in Potassium–Nitroimidazoles Collisions: An Experimental and Theoretical Work. *Int. J. Mol. Sci.* **2019**, *20*, 6170

(2) Meißner, R.; Kocisek, J.; Feketeová, L.; Fedor, J.; Fárník, M.; Limão-Vieira, P.; Illenberger, E.; Denifl, S. Low-Energy Electrons Transform the Nimorazole Molecule Into a Radiosensitiser. *Nat. Commun.* **2019**, *10*, 2388

(3) Itälä, E.; Myllynen, H.; Niskanen, J.; Gonzalez-Vazquez, J.; Wang, Y.; Trinh Ha, D.; Paul Denifl, S.; Kukk, E. Controlling NO Production Upon Valence Ionization of Nitroimidazoles. *J. Phys. Chem. A* **2019**, *123*, 3074–3079

(4) Cartoni, A.; Casavola, A. R.; Bolognesi, P.; Castrovilli, M. C.; Catone, D.; Chiarinelli, J.; Richter, R.; Avaldi, L. Insights into 2- and 4(5)-Nitroimidazole Decomposition into Relevant Ions and Molecules Induced by VUV Ionization. *J. Phys. Chem. A* **2018**, *122*, 4031–4041

(5) Pandeti, S.; Feketeová, L.; Reddy, T. J.; Abdoul-Carime, H.; Farizon, B.; Farizon, M.; Märk, T. D. Nitroimidazolic Radiosensitizers Investigated by Electrospray Ionization Time-of-Flight Mass Spectrometry and Density Functional Theory. *RSC Adv.* **2017**, *7*, 45211–45221

(6) Itälä, E.; Tanzer, K.; Granroth, S.; Kooser, K.; Denifl, S.; Kukk, E. Fragmentation Patterns of 4(5)-Nitroimidazole and 1-Methyl-5-Nitroimidazole – The Effect of the Methylation. *J. Mass Spectrom.* **2017**, *52*, 770–776

(7) Bolognesi, P.; Casavola, A. R.; Cartoni, A.; Richter, R.; Markus, P.; Borocci, S.; Chiarinelli, J.; Tošić, S.; Sa'adeh, H.; Masič, M. et al. Communication: Position Does Matter: The Photofragmentation of the Nitroimidazole Isomers. *J. Chem. Phys.* **2016**, *145*, 191102

(8) Feketeová, L.; Plekan, O.; Goonewardane, M.; Ahmed, M.; Albright, A. L.; White, J.; O´Hair, R. A. J.; Horsman, M. R.; Wang, F.; Prince, K. C. Photoelectron Spectra and Electronic Structures of the Radiosensitizer Nimorazole and Related Compounds. *J. Phys. Chem. A* **2015**, *119*, 9986–9995

(9) Feketeová, L.; Postler, J.; Zavras, A.; Scheier, P.; Denifl, S.; O'Hair, R. A. J. Decomposition of Nitroimidazole Ions: Experiment and Theory. *Phys. Chem. Chem. Phys.* **2015**, *17*, 12598–12607

(10) Tanzer, K.; Feketeová, L.; Puschnigg, B.; Scheier, P.; Illenberger, E.; Denifl, S. Reactions in Nitroimidazole Triggered by Low-Energy (0-2eV) Electrons: Methylation at N1-H Completely Blocks Reactivity. *Angew. Chem. Int. Ed.* **2014**, *53*, 12240–12243

(11) Murata, R.; Tsujitani, M.; Horsman, M. R. Enhanced Local Tumour Control after Single or Fractionated Radiation Treatment Using the Hypoxic Cell Radiosensitizer Doranidazole. *Radiother. Oncol.* **2008**, *87*, 331–338

(12) Overgaard, J.; Sand Hansen, H.; Andersen, A. P.; Hjelm-Hansen, M.; Jørgensen, K.; Sandberg, E.; Berthelsen, A.; Hammer, R.; Pedersen, M. Misonidazole Combined with Split-Course Radiotherapy in the Treatment of Invasive Carcinoma of Larynx and Pharynx: Report from the DAHANCA 2 Study. *Int. J. Radiat. Oncol. Biol. Phys.* **1989**, *16*, 1065–1068

(13) Overgaard, J.; Hansen, H. S.; Overgaard, M.; Bastholt, L.; Berthelsen, A.; Specht, L.; Lindeløv, B.; Jørgensen, K. A Randomized Double-Blind Phase III Study of Nimorazole as a Hypoxic Radiosensitizer of Primary Radiotherapy in Supraglottic Larynx and Pharynx Carcinoma. Results of the Danish Head and Neck Cancer Study (DAHANCA) Protocol 5-85. *Radiother. Oncol.* **1998**, *46*, 135–146

(14) Kelly, C. G. Radiotherapy in the Management of Orofacial Cancer, *Maxillofacial Surgery*, third edition; Churchill Livingstone 2017; 324–338

(15) Howard-Flanders, P.; Alper, T. The Sensitivity of Microorganisms to Irradiation under Controlled Gas Conditions. *Radiat. Res.* **1957**, *7*, 518–540

(16) Edwards, D. I. Reduction of Nitroimidazoles In Vitro and DNA Damage. *Biochem. Pharmacol.* **1986**, *35*, 53–58

(17) Oronsky, B. T.; Knox, S. J.; Scicinski, J. Six Degrees of Separation: The Oxygen Effect in the Development of Radiosensitizers. *Transl. Oncol.* **2011**, *4*, 189–198

(18) Oronsky, B. T.; Knox, S. J.; Scicinski, J. J. Is Nitric Oxide (NO) the Last Word in Radiosensitization?: A Review. *Transl. Oncol.* **2012**, *5*, 66–71

(19) Horsman, M. R.; Lindegaard, J. C.; Grau, C.; Nordsmark, M.; Alsner, J.; Overgaard, J. Dose-Response Modifiers in Radiation Therapy, *Clinical Radiation Oncology*, fourth edition; Elsevier: Philadelphia, 2016; 51–62.e3

(20) Kukk, E.; Ha, D. T.; Wang, Y.; Piekarski, D. G.; Diaz-Tendero, S.; Kooser, K.; Itälä, E.; Levola, H.; Alcamí, M.; Rachlew, E. *et al.* Internal Energy Dependence in X-Ray-Induced Molecular Fragmentation: An Experimental and Theoretical Study of Thiophene. *Phys. Rev. A* **2015**, *91*, 043417

(21) Suga, S.; Sekiyama, A. Photoelectron Spectroscopy; Springer, Berlin Heidelberg, 2014

(22) Eland, J. H. *Photoelectron Spectroscopy. An Introduction to Ultraviolet Photoelectron Spectroscopy in the Gas Phase*, second edition; Butterworths: Southampton, 1984

(23) Neese, F. Software Update: the ORCA Program System, Version 4.0. *WIREs Comput. Mol. Sci.* **2017**, e1327

(24) Perdew, J. P.; Burke, K.; Ernzerhof, M. Generalized Gradient Approximation Made Simple. *Phys. Rev. Lett.* **1996**, *77*, 3865–3868

(25) Weigend, F.; Ahlrichs, R. Balanced Basis Sets of Split Valence, Triple Zeta Valence and Quadruple Zeta Valence Quality for H to Rn: Design and Assessment of Accuracy. *Phys. Chem. Chem. Phys.* **2005**, *7*, 3297–3305

(26) Weigend, F. Accurate Coulomb-Fitting Basis Sets for H to Rn. *Phys. Chem. Chem. Phys.* **2006**, *8*, 1057–1065

(27) Kukk, E.; Kooser, K.; Ha, D. T.; Granroth, S.; Nõmmiste, E. VUV-Induced Dissociation of Methylchlorosilanes, Studied by ElectronIon Coincidence Spectroscopy. *J. Phys. B* **2010**, *43*, 065103

(28) Brown, J. M. Selective Radiosensitization of the Hypoxic Cells of Mouse Tumors with the Nitroimidazoles Metronidazole and Ro 7-0582. *Radiat. Res.* **1975**, *64*, 633–647

TOC Graphic